PAPER

A simple method for the preparation of a nickel selenide and cobalt selenide mixed catalyst to enhance bifunctional oxygen activity for Zn–air batteries†

Li-Juan Peng,[ab] Jie-Ping Huang,[a] Qiu-Ren Pan,[a] Ying Liang,[a] Na Yin,[a] Hang-Chang Xu[a] and Nan Li [ID] *[a]

Developing a low-cost, simple, and efficient method to prepare excellent bifunctional electrocatalysts toward the oxygen reduction reaction (ORR) and oxygen evolution reaction (OER) is critical in rechargeable zinc–air batteries. Non-stoichiometric $M_{0.85}Se$ (M = Ni or Co) nanoparticles are synthesized and modified on nitrogen-doped hollow carbon sphere (NHCS). The NHCS loaded $Ni_{0.85}Se$ ($Ni_{0.85}Se$-NHCS) with rich Ni^{3+} presents higher OER activity, whereas the NHCS-loaded $Co_{0.85}Se$ ($Co_{0.85}Se$-NHCS) with abundant Co^{2+} displays better ORR activity, respectively. When $Co_{0.85}Se$-NHCS is mixed with $Ni_{0.85}Se$-NHCS in a mass ratio of 1 : 1, the resulting mixture ($Ni_{0.85}Se/Co_{0.85}Se$-NHCS-2) shows better ORR and OER dual catalytic functions than a single selenide. Moreover, zinc–air batteries equipped with $Ni_{0.85}Se/Co_{0.85}Se$-NHCS-2 as the oxygen electrode catalyst exhibit excellent charge and discharge performance as well as improved stability over precious metals. This work has developed a simple and effective method to prepare excellent bifunctional electrocatalysts for ORR and OER, which is beneficial for the practical large-scale application of zinc–air batteries.

Introduction

Due to the exhaustion of fossil fuel energy and environmental deterioration, the development of efficient, clean, and sustainable energy storage technology has attracted worldwide attention.[1–3] Zinc–air batteries are considered an ideal candidate for renewable energy technologies due to their high power density, high output capacity, long-term stability, and environmental friendliness.[4–6] The performance of rechargeable zinc–air batteries depends mainly on the properties of the oxygen reduction reactions (ORR) and oxygen evolution reactions (OER) that occur during discharging or charging on the cathode, respectively.[7–9] Usually, noble metal Pt-based and RuO_2 materials are considered as superior catalysts for ORR and OER, respectively, to accelerate the sluggish kinetics of the reaction.[10–13] However, due to the price, long-term stability, and limited reserves of noble metal catalysts, the practical application of rechargeable Zn–Air batteries will be severely limited when noble metals are used as cathode catalysts to achieve the dual function

of ORR and OER.[14–17] Therefore, the development of low-cost, easy-to-prepare, durable, and dual-functional non-precious metal catalysts with high ORR and OER activities has become the key to achieve the practical application of Zn–Air batteries.

The transition metal selenide as the earth-abundant and low-cost materials have made great efforts to replace precious metal electrocatalysts to achieve durability and efficiency in electrochemical energy storage.[18–20] Compared with transition metal oxides and sulfides, transition metal selenides have greater intrinsic metallic conductivity, which facilitates electron transfer in the electrocatalytic process.[21–23] Especially, the non-stoichiometric transition metal selenides such as $Co_{0.85}Se$ and $Ni_{0.85}Se$ exhibit excellent electrocatalysis toward OER and ORR on account of the non-stoichiometric configuration, and corresponding varied metallic valence states and metal vacancies.[24,25] Besides, Ni^{3+} in $Ni_{0.85}Se$ and Co^{3+} in $Co_{0.85}Se$ are beneficial to the formation of NiOOH or CoOOH,[26,27] ascribing to the real active site during the OER process, whereas Ni^{2+} and Co^{2+} are attributed to the active site for ORR.[28]

Owing to the poor electronic conduction, the transition metal selenides usually anchor in the high electronic conduction such as carbon-based materials, which effectively are exposed to the more active sites and achieve long-term stability in the electrocatalysis process.[29,30] Besides, to further improve the catalytic activity of carbon-based electrocatalysts, the electrocatalytic activity of carbon materials can be enhanced by doping with

[a]School of Chemistry and Chemical Engineering, Guangzhou Key Laboratory for Clean Energy and Materials, Guangzhou University, Guangzhou 510006, China. E-mail: nanli@gzhu.edu.cn

[b]College of Chemistry and Materials Science, Jinan University, Guangzhou 510632, China

† Electronic supplementary information (ESI) available. See DOI: 10.1039/d1ra02861h

heteroatoms. For example, Gui *et al.*[28] reported the $Co_{0.85}Se$ nanoparticle encapsulating the 1D nitrogen-doped carbon nanofibers (CNFs), which exhibited excellent bifunctional electrocatalysis activity toward OER and ORR and superior electrochemical stability because of the synergistic effect between $Co_{0.85}Se$ and N-doped CNFs heterostructures and sufficient electrochemically active site. Because of the nitrogen-doped mesoporous carbon (NMC) modifying the CoSe, CoSe@NMC displays excellent performance for OER and ORR.[31] However, the transition metal selenides practically gain the bifunctional electrocatalysis by many complicated strategies consisting of the construct of heterointerfaces,[32] engineering of the defect,[25] and formation of electronic interaction[33,34] to optimize the adsorption/desorption of reaction intermediates. Therefore, it is important to develop an excellent, durable, and inexpensive bifunctional electrocatalyst based on transition metal selenides for ORR and OER by a simple and easy method, which really contributes to the practical application of zinc–air batteries.

Because of the high electrocatalytic activity of nitrogen-doped hollow carbon spheres, we synthesized mixed $M_{0.85}Se$ (M = Ni or Co) nanoparticles modified on nitrogen-doped hollow carbon spheres ($Ni_{0.85}Se$-NHCS mixed with $Co_{0.85}Se$-NHCS) as OER/OER electrocatalytic materials. The simple physical mixing method simplified the preparation process and reduced the preparation cost. The nitrogen-doped hollow carbon sphere facilitated the mass/charge transfer and reduced aggregation of the nanoparticle during the electrocatalysis process. Due to the suitable ratio of Ni^{3+}/Ni^{2+} and Co^{3+}/Co^{2+}, $Ni_{0.85}Se$-NHCS had better catalytic activity for OER, while $Co_{0.85}Se$-NHCS had higher performance for ORR. The mixture $Ni_{0.85}Se/Co_{0.85}Se$-NHCS-2 displayed the superior electrocatalytic performance for both ORR and OER than the $Ni_{0.85}Se$-NHCS or $Co_{0.85}Se$-NHCS alone because of the synergistic effect between $Ni_{0.85}Se$-NHCS and $Co_{0.85}Se$-NHCS. Compared with the zinc–air batteries using Pt/C and RuO_2 hybrid catalysts, the batteries using $Ni_{0.85}Se/Co_{0.85}Se$-NHCS-2 hybrid catalysts showed similar charge and discharge performance and better long-term stability. This work can provide a simple and low-cost method for the design and development of ORR/OER bifunctional electrocatalysts, which is beneficial for the practical application of zinc–air batteries.

Experimental section

Chemicals

$NiCl_2 \cdot 6H_2O$, $CoCl_2 \cdot 6H_2O$, formaldehyde, resorcinol, hexadecyl trimethyl ammonium bromide (CTAB) and tetraethoxysilane (TEOS) were purchased from Aladdin Reagent (Shanghai) Co., Ltd. Ammonia solution (25%) and ethanol were provided from Tianjin Baishi Chemical Co., Ltd. Hydrazine hydrate ($N_2H_4 \cdot H_2O$, 80%) were supplied from Tianjin Damao Chemical Reagent Factory.

Synthesis of NHCS

The synthesis of the nitrogen-doped hollow carbon sphere (NHCS) was performed following the hard template method.[27] 0.5 g of resorcinol was dissolved in 70 mL of ethanol and 10 mL of distilled water. Then 3 mL of ammonia solution added to the

above solution under magnetic stirring. Subsequently, 0.72 mL of formaldehyde and 2.8 mL of TEOS were dropped in five minutes. For forming more mesoporous in the carbon sphere, 1.5 mL of TEOS was added to the above-mixed solution after 6 hours. The products were filtered and dried at 50 °C overnight before carbonation at 800 °C for 2 hours. Finally, NHCS was gained after performing 6 M of NaOH solution at 70 °C for 6 hours to etching silica spheres.

Synthesis of $Ni_{0.85}Se$-NHCS and $Co_{0.85}Se$-NHCS

50 mg of NHCS, 59.4 mg of $NiCl_2 \cdot 6H_2O$, 59.4 mg of $NaSeO_3$, and 50 mg CTAB were dissolved in 60 mL of distilled water under ultrasonic operation for 1 hour. Subsequently, 8 mL of $N_2H_4 \cdot H_2O$ was dropped in the above solution and transferred to a Teflon-lined autoclave and kept at 140 °C in an oven for 24 h. After filtered and washed with distilled water, the product was dried at 50 °C for 12 hours. Eventually, the product was performed further calcination in N_2 atmosphere at 600 °C for 2 hours. The loading masses of $Ni_{0.85}Se$ and $Co_{0.85}Se$ were calculated to be about 1.29 mg per gram of carbon sphere based on the addition of metal salts and carbon spheres. The synthesis of $Co_{0.85}Se$-NHCS was following the above process and the difference was that $CoCl_2 \cdot 6H_2O$ was used instead of $NiCl_2 \cdot 6H_2O$. 50% Ni-$Co_{0.85}Se$-NHCS was prepared by a similar co-deposition method as a contrast. The mass of both $CoCl_2 \cdot 6H_2O$ and $NiCl_2 \cdot 6H_2O$ were 27 mg, other conditions remained the same.

Mixing of $Ni_{0.85}Se$-NHCS and $Co_{0.85}Se$-NHCS

The above-prepared $Ni_{0.85}Se$-NHCS and $Co_{0.85}Se$-NHCS were mixed with the mass radio of 1 : 2, 1 : 1 and 2 : 1, which was labeled as $Ni_{0.85}Se/Co_{0.85}Se$-NHCS-1, $Ni_{0.85}Se/Co_{0.85}Se$-NHCS-2 and $Ni_{0.85}Se/Co_{0.85}Se$-NHCS-3, respectively.

Characterization

The crystal structure's information of the samples was gained *via* X-ray diffraction (XRD, PANalytical, PW3040/60 diffractometer) with Cu Kα radiation (λ = 0.15418 nm). The surface chemical state of the above samples was tested by X-ray photoelectron spectroscopy (XPS, ESCALab 250) and performed by XPSPEAK software. The surface microstructure and morphology of the above-prepared samples were examined by field-emission scanning electron microscopy (FESEM, JEOL JSM-7001F) and transmission electron microscopy (TEM, JEM2010-HR). The BET specific surface area of the above samples was measured by nitrogen adsorption–desorption isotherm (Micromeritics ASAP 2460) and pore size distribution used the BJH desorption model.

Electrochemical measurements

The catalyst ink was contained with 3 mg of catalyst, 500 μL of isopropanol, 500 μL of distilled water, and 20 μL of Nafion®resin solutions (5.0 wt%). And then, 5 μL of catalyst ink was dropped on the glassy carbon rotating disk electrode (RDE,

0.126 cm^2) or glassy carbon ring rotating disk electrode (RRDE, 0.196 cm^2). Finally, the above catalyst was dried in the air.

The ORR and OER catalytic activity was examined on CHI 760e electrochemical workstation (Shanghai, Chenhua) using a three-electrode system, where the RDE (0.126 cm^2) with Ni$_{0.85}$Se-NHCS or Co$_{0.85}$Se-NHCS film as the working electrode, the Hg/HgO as the reference electrode and a carbon rod of spectral purity as a counter electrode. But the electron transfer numbers and hydrogen peroxide yield was used in an AMETEK Princeton Applied Research PMC 2000A equipped with an RRDE as a working electrode. All the ORR and OER catalytic activity were performed in O$_2$-saturated 0.1 M KOH electrolyte.

The electrochemical surface area (ECSA) was gained by CV measurement in the non-faraday current region by varying the scan rates from 2 mV s^{-1} to 10 mV s^{-1}. The current is positively related to the scan rate:

$$I_c = C_{dl} \times v$$

I_c represents the non-faraday current; C_{dl} represents the electrochemical double-layer capacitance; v means the scan rates. The ECSA is further gained by normalizing C_{dl} with the special capacitance of 40 μF cm^{-2} for a flat surface, which would apply to the turnover frequency (TOF) calculations. According to the previous literature,[35] TOF for OER was calculated by the following equation:

$$TOF = \frac{turn\ over\ the\ number\ of\ O_2}{N \times A_{ECSA}}$$

Thereinto, N is the number of active sites

$$\text{Turn over the number of } O_2 = \frac{j \times 1\ C\ s^{-1}}{1000\ mA} \times \frac{1\ mol}{96\ 485.3\ C}$$
$$\times \frac{1\ mol\ O_2}{4\ mol}$$
$$\times \frac{6.022 \times 10^{23}\ O_2\ molecules}{1\ mol\ O_2}$$
$$= j \times 1.56$$
$$\times 10^{15}\ molecules\ per\ mA\ per\ s$$

Since the real surface active site was unknown, we evaluated Co and Ni in the surface as the active site. The active sites per real surface area are shown in the following equation:

$$\text{Number of active sites}(Co_{0.85}Se\text{-}NHCS)$$
$$= \left(\frac{2\ atom\ per\ unit\ cell}{59.8\ \text{Å}^3\ per\ unit\ cell}\right)^{\frac{2}{3}}$$

$$\text{Number of active sites}(Ni_{0.85}Se\text{-}NHCS)$$
$$= \left(\frac{2\ atom\ per\ unit\ cell}{60.1\ \text{Å}^3\ per\ unit\ cell}\right)^{\frac{2}{3}}$$

The number of active sites of Ni$_{0.85}$Se/Co$_{0.85}$Se-NHCS-2 is the average of the Ni$_{0.85}$Se-NHCS and Co$_{0.85}$Se-NHCS. Besides, the unit cell of Ni$_{0.85}$Se and Co$_{0.85}$Se are shown in Fig. S1,† according to the standard crystal card of Ni$_{0.85}$Se (JCPDS No. 18-0888) and Co$_{0.85}$Se (JCPDS No. 52-1008), respectively.

The electron transfer number (n) and hydrogen peroxide yield calculate the following equation:

$$n = \frac{4 \times I_D}{I_D + I_R/N}$$

$$H_2O_2\% = 200 \times \frac{I_R/N}{I_R/N + I_D}$$

I_D and I_R represent the disk current and the ring current of RRDE. N means the collection efficiency of the ring (34%).

The Zn–air battery measurement was carried out on CHI 760e electrochemical workstation (Shanghai, Chenhua) at room temperature. Zinc foil was worked as the anode and the catalyst coating in carbon paper was performed as the cathode with a geometric area of 1 cm^2. 5 mg of catalyst was dispersed into 20 μL of 5% Nafion solution, 300 μL water, and 700 μL of isopropanol solution. The electrolyte contained 6 M KOH and 0.2 M Zn(Ac)$_2$. As a reference, 2.5 mg of 20% Pt/C and 2.5 mg of RuO$_2$ were performed with the above-same process.
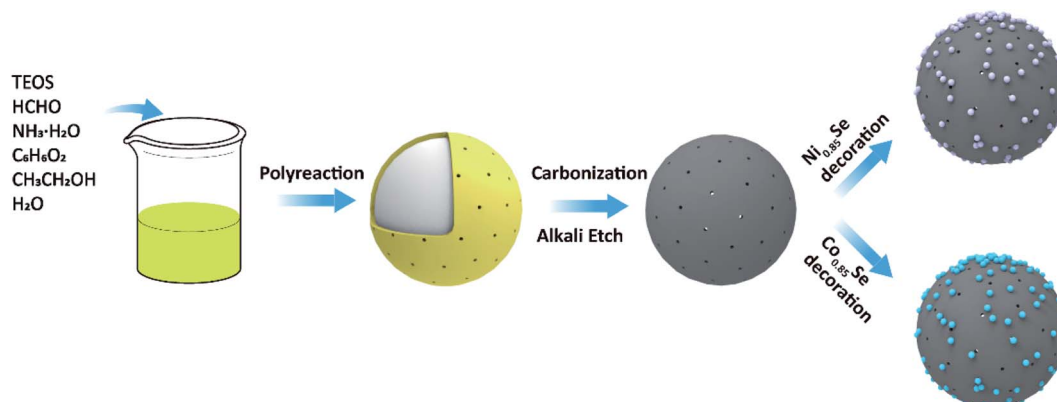

Fig. 1 The schematic of the preparation process of M$_{0.85}$Se-NHCS (M = Ni, Co).

Results and discussion

The synthesis process of $M_{0.85}Se$-NHCS (M = Ni, Co) is shown in Fig. 1. Initially, the phenolic resin was coated on the SiO_2 spheres by polyreaction at room temperature. The yellow precursors collecting by filtration were carbonized at 800 °C for 2 hours in the nitrogen atmospheres. After the SiO_2 removal, the nitrogen-doped hollow spheres (NHCS) were decorated with $M_{0.85}Se$ (M = Ni, Co) nanoparticles. The $M_{0.85}Se$-NHCS (M = Ni, Co) was successfully synthesized following the above process.

The micromorphology and microstructure of the prepared catalysts $Ni_{0.85}Se$-NHCS and $Co_{0.85}Se$-NHCS were carried out by scanning electron microscopy (SEM) and transmission electron microscopy (TEM). As shown in Fig. S2a and b,† the NHCS with an average diameter of 400 nm size exhibited a roughly spherical structure. As shown in the results of SEM (Fig. S2c–f†) and TEM (Fig. 2a and d), the NHCS was uniformly immobilized with tiny nanoparticles ($Ni_{0.85}Se$ or $Co_{0.85}Se$) abounding on the surface after hydrothermal reaction. For 50% Ni-$Co_{0.85}Se$, it can be seen the $Ni_{0.85}Se$ and $Co_{0.85}Se$ nanoparticles were co-deposited on the NHCS uniformly (Fig. S2j and k†). Furthermore, high-resolution transmission electron microscopy (HRTEM) was used to analyze the microstructure of the nanoparticles and to confirm the composition of the nanoparticles. As shown in Fig. 2b, the lattice fringes with interplanar width of 2.70 Å and 1.18 Å corresponded to the (101) and (110) planes of $Ni_{0.85}Se$, respectively. Besides, the crystal interplanar spacings of 2.69 Å corresponding to the (101) planes in Fig. 2e indicated the existence of the $Co_{0.85}Se$ crystal. The EDX mappings of $Ni_{0.85}Se$-NHCS in Fig. 2c revealed the homogeneous distribution of Ni, Se, N, and C element. Similarly, the element of Co, Se, N, and C were uniformly distributed on the $Co_{0.85}Se$-NHCS in Fig. 2f. Furthermore, the EDX results implied the successful synthesis of non-stoichiometric $Co_{0.85}Se$ and $Ni_{0.85}Se$ (Fig. S3 and S4†). As we all know, the non-stoichiometric materials

provide numerous active sites because of their specific stoichiometry of metal vacancies which makes them abundant unsaturated atoms and boost the ORR and OER activities.[24,28] Besides, the presence of the nitrogen component further demonstrated that the successful doping of nitrogen on the hollow carbon spheres, which changed the charge distribution of the carbon material and facilitated the absorption and desorption of oxygen in ORR or OER process.[36,37]

X-ray diffraction (XRD) patterns revealed the crystal structure information of the as-prepared samples. In Fig. 3a, the XRD patterns of $Co_{0.85}Se$-NHCS and $Ni_{0.85}Se$-NHCS were in agreement well with the standard crystal card of $Ni_{0.85}Se$ (JCPDS No. 18-0888) and $Co_{0.85}Se$ (JCPDS No. 52-1008), respectively. The diffraction peak positions of 33.15°, 44.95°, and 50.49° were accountable with (101), (102), and (110) crystal planes of hexagonal crystalline $Ni_{0.85}Se$, correspondingly. Similarly, the diffraction peak positions at 33.26°, 44.74°, and 50.56° were related to (101), (102), and (110) crystal planes of hexagonal crystalline $Co_{0.85}Se$. The XRD patterns consistent with the standard card further demonstrated the successful synthesis of $Co_{0.85}Se$ and $Ni_{0.85}Se$. Besides, as shown in Fig. S5a,† when the $Co_{0.85}Se$-NHCS and $Ni_{0.85}Se$-NHCS were mixed with the mass radio of 1 : 1, the XRD pattern of $Co_{0.85}Se/Ni_{0.85}Se$-NHCS-2 was unquestionably unchanged. As shown in Fig. 3b, the Raman peaks at 384 cm^{-1} were ascribed to Se–Se librational and stretching vibrations of the NiSe.[38–40] The characteristic peaks at 188 cm^{-1} and 678 cm^{-1} were indexed to the A_g and A_{1g} of CoSe, respectively.[41,42] Additionally, there were distinctive peaks at 1335 cm^{-1} (D band) and 1590 cm^{-1} (G band) attributed to sp^3 and sp^2 hybridized carbons.[43] The intensity ratios of D band and G band of $Ni_{0.85}Se$-NHCS, $Co_{0.85}Se$-NHCS, $Co_{0.85}Se/Ni_{0.85}Se$-NHCS-2 and NHCS (Fig. S5b†) were nearly 0.99, 0.98, 0.99, and 0.88, respectively. Raman results showed that the NHCS possessed a high degree of graphitization, resulting in high electrical conductivity.[44] After combined with $Co_{0.85}Se$ or
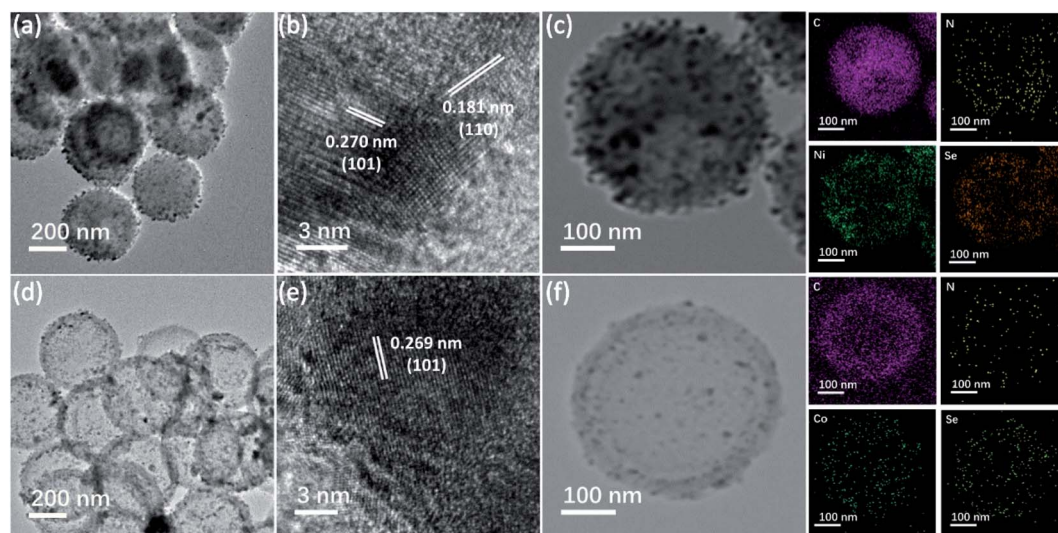

Fig. 2 (a and d) The TEM images, (b and e) high-resolution transmission electron microscopy image, and (c and f) EDX mappings of $Ni_{0.85}Se$-NHCS and $Co_{0.85}Se$-NHCS, respectively.
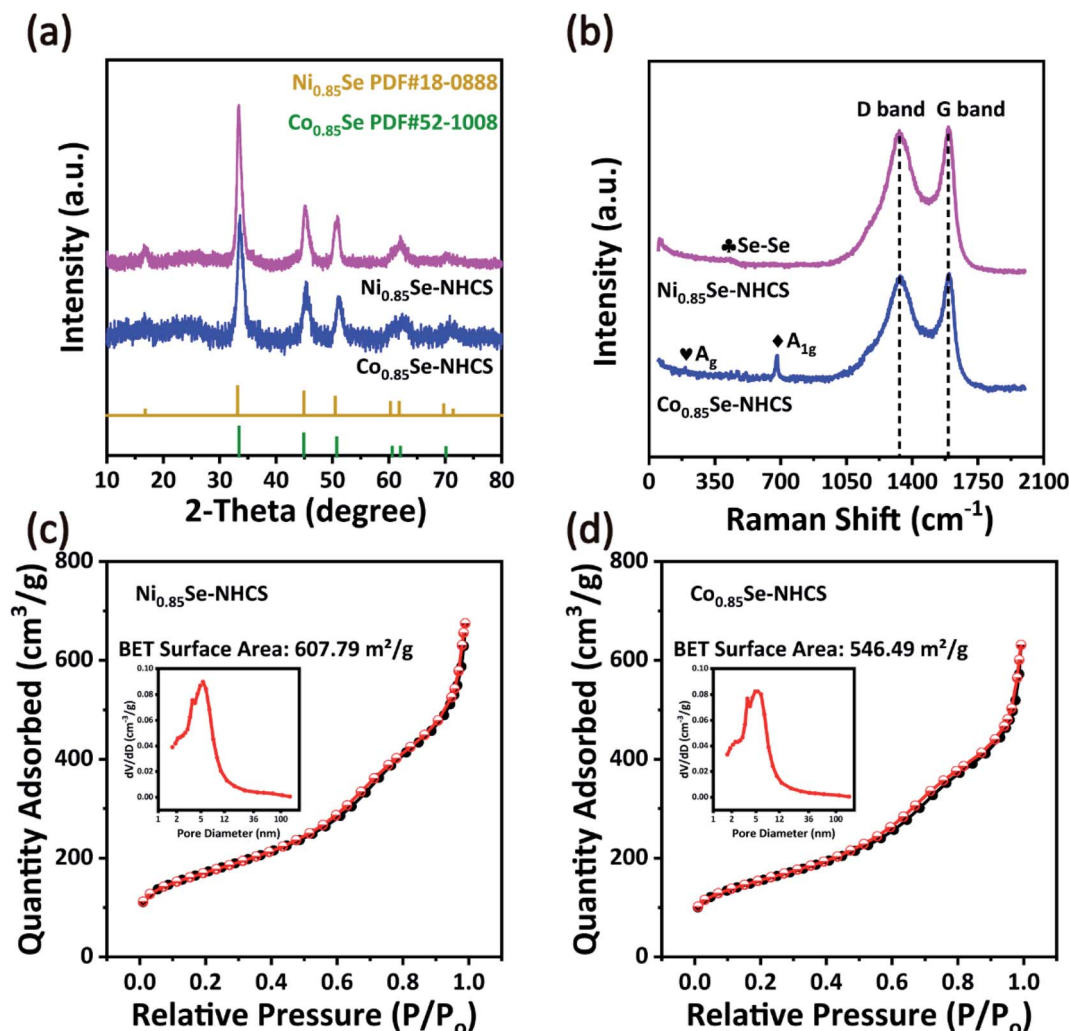
Fig. 3 (a) The XRD patterns and (b) Raman patterns of $Ni_{0.85}Se$-NHCS and $Co_{0.85}Se$-NHCS. (c) N_2 adsorption/desorption isotherms of $Ni_{0.85}Se$-NHCS (inset: pore size distribution) and (d) N_2 adsorption/desorption isotherms of $Co_{0.85}Se$-NHCS (inset: pore size distribution).

$Ni_{0.85}Se$, the $Ni_{0.85}Se$-NHCS, $Co_{0.85}Se$-NHCS, and $Co_{0.85}Se/$ $Ni_{0.85}Se$-NHCS-2 had abundant defect because of the existence of the non-stoichiometric $M_{0.85}Se$ (M = Ni or Co) nanoparticle, providing the more active site to boost the ORR and OER activities, which is consistent with previous literature.[45–47] The N_2 adsorption/desorption isotherms and corresponding pore size distribution of $Ni_{0.85}Se$-NHCS, $Co_{0.85}Se$-NHCS, and $Co_{0.85}Se/Ni_{0.85}Se$-NHCS-2 were revealed in Fig. 3c, d, and S5,† respectively. The specific surface area of the $Ni_{0.85}Se$-NHCS, $Co_{0.85}Se$-NHCS, and $Co_{0.85}Se/Ni_{0.85}Se$-NHCS-2 was 607.79, 546.49, and 554.67 $m^2\,g^{-1}$, respectively. Also, the N_2 adsorption/ desorption isotherms curves of the above samples had a hysteresis loop at a relative pressure between 0.5 and 0.9. These curves belonged to IV profiles and carried out numerous mesoporous structures in these catalysts. Besides, the pore size distribution curves demonstrated that these catalysts retained rich micropores and mesopores. The abundant porous structures of samples accelerated the mass and charge transfer and provided a large amount of specific surface area, which was conducive to the high performance of oxygen reduction and oxygen evolution reactions.[48]

The surface chemical state and element composition of the catalyst was carried out by XPS analysis in Fig. 4. The survey spectrum of the $Ni_{0.85}Se$-NHCS presented the existence of C, N, O, Se and Ni elements, while $Co_{0.85}Se$-NHCS displayed the coexistence of C, N, O, Se and Co elements (Fig. S6a†). The O element was attributed to the exposure to air, which was consistent with the description in the literature.[32] As displayed in Fig. 4a, the Ni 2p spectrum was deconvoluted into two main peaks along with two satellite peaks. The peak located at 853.6 eV of Ni $2p_{3/2}$ and 870.9 eV of Ni $2p_{1/2}$ were attributed to Ni^{2+} of $Ni_{0.85}Se$-NHCS, and the peak located at 856 eV of Ni $2p_{3/2}$ and 873.9 eV of Ni $2p_{1/2}$ were ascribed to Ni^{3+} of $Ni_{0.85}Se$-NHCS.[49,50] Similarly, the high-resolution spectrum of Co 3p was split into two main peaks and two satellite peaks in Fig. 4b. The peaks situated at 778.6 eV for Co $2p_{3/2}$ and 793.78 eV for Co $2p_{1/2}$ demonstrated the existence of Co^{3+} in $Co_{0.85}Se$-NHCS, and the peaks situated at 781.1 eV for Co $2p_{3/2}$ and 797.1 eV for Co $2p_{1/2}$ corresponded to Co^{2+} in $Co_{0.85}Se$-NHCS.[51–54] As the
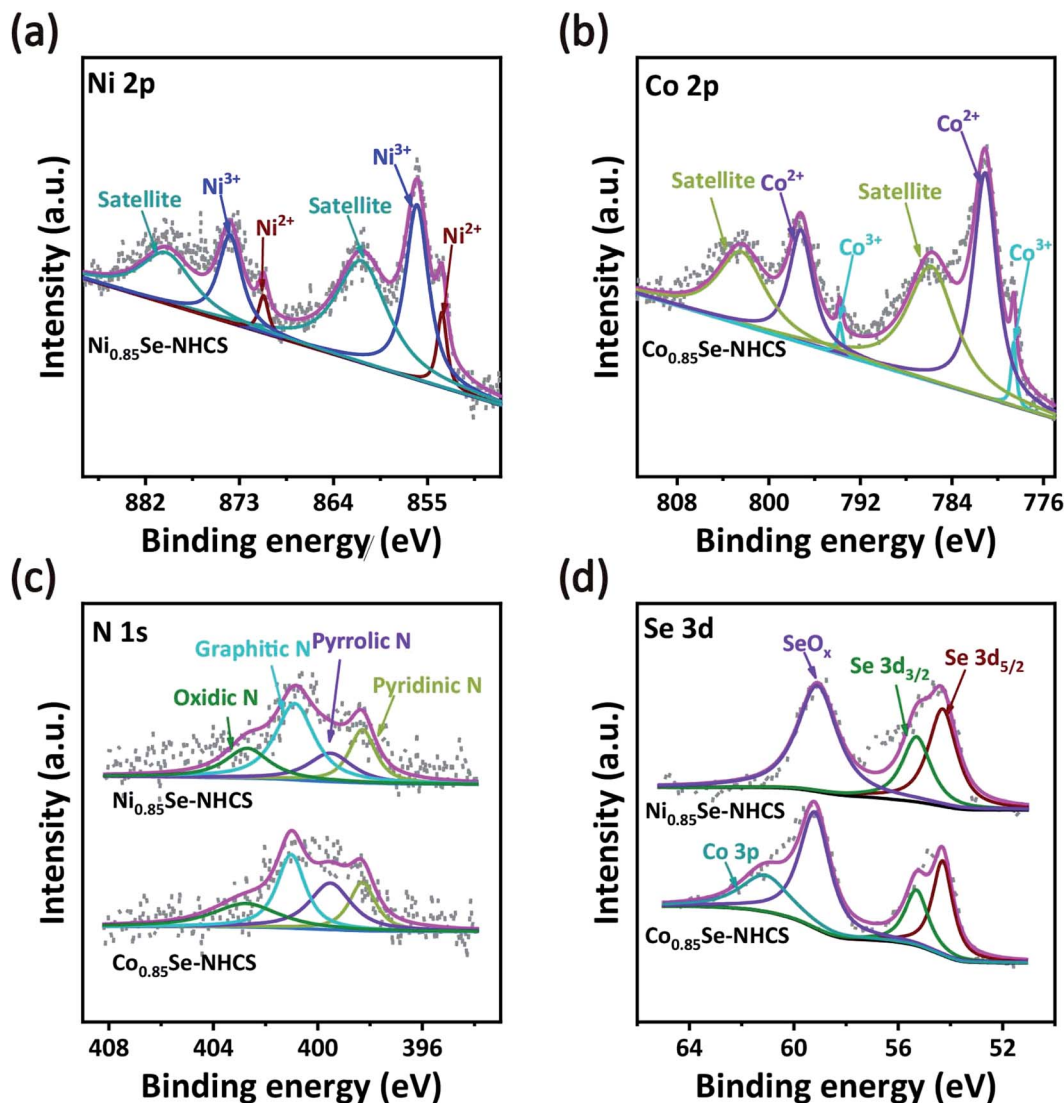
Fig. 4 High-resolution XPS of (a) Ni 2p, (b) Co 2p, (c) N 1s and (d) Se 3d of $Ni_{0.85}Se$-NHCS and $Co_{0.85}Se$-NHCS.

deconvolution of Ni 2p, the Ni^{3+}/Ni^{2+} ratio of $Ni_{0.85}Se$-NHCS was 5.55, implying that the Ni^{3+} content was much higher than that of Ni^{2+}. It has been reported that Ni^{3+} was considered the active site for OER by absorbing OH^{-} owing to the formation of NiOOH.[12,26] So it can be reasonably inferred that $Ni_{0.85}Se$-NHCS was favorable to OER. On the other hand, the Co 2p spectrum showed that the Co^{3+}/Co^{2+} ratio of $Co_{0.85}Se$-NHCS was 0.06. It indicates a large amount of Co^{2+}, which was considered to favor ORR.[28] In the spectrum of Fig. 4c, the N 1s peaks of $Ni_{0.85}Se$-NHCS and $Co_{0.85}Se$-NHCS were split into four main peaks ascribed to pyridinic N (398.3 eV), pyrrolic N (399.5 eV), graphitic N (400.9 eV), and oxidic N (402.8 eV), respectively.[55] As revealed in the Fig. 4d, the Se 3d spectrums of $Ni_{0.85}Se$-NHCS and $Co_{0.85}Se$-NHCS were split into Se $3d_{5/2}$ (54.3 eV), Se $3d_{3/2}$ (55.75 eV), and SeO_x (59.2 eV).[56] The existence of SeO_x was attributable to exposure to air. So the selenium of transition metal selenides was oxidized to selenites, then to selenates. The adsorption of selenate on the surface of the sample promoted

the oxygen evolution reaction, strengthening the OER intermediates bond.[57] Interestingly, compared with $Ni_{0.85}Se$-NHCS, the extra peak located at 61.61 eV in the Se spectrum of $Co_{0.85}Se$-NHCS was ascribed to Co 3p, which was consistent with the previous literature.[55] Furthermore, the C 1s spectrums of $Ni_{0.85}Se$-NHCS and $Co_{0.85}Se$-NHCS were deconvoluted into four main peaks corresponding to the C=C (248.8 eV), C-C (285.6 eV), C=N (286.9 eV), and C=O (289.4 eV) in Fig. S6b.†

The single NHCS without metal selenide only showed very weak ORR and OER activity (Fig. S7†). After $M_{0.85}Se$ (M = Ni, Co) was decorated on NHCS, the ORR performance of catalysts had been greatly improved due to the intrinsic catalytic quality of $Ni_{0.85}Se$ and $Co_{0.85}Se$ (Fig. 5). As shown in Fig. 5a, the $Ni_{0.85}Se$/$Co_{0.85}Se$-NHCS-2 exhibited excellent ORR activities with the onset potential of 0.90 V, a half-wave potential of 0.77 V, and a limiting current density of 4.66 mA cm^{-2}, closing those of the $Co_{0.85}Se$-NHCS (E_{onset} = 0.89 V, $E_{1/2}$ = 0.76 V and J_L = 4.67 mA cm^{-2}) and exceeding the $Ni_{0.85}Se$-NHCS (E_{onset} = 0.79 V, $E_{1/2}$ =
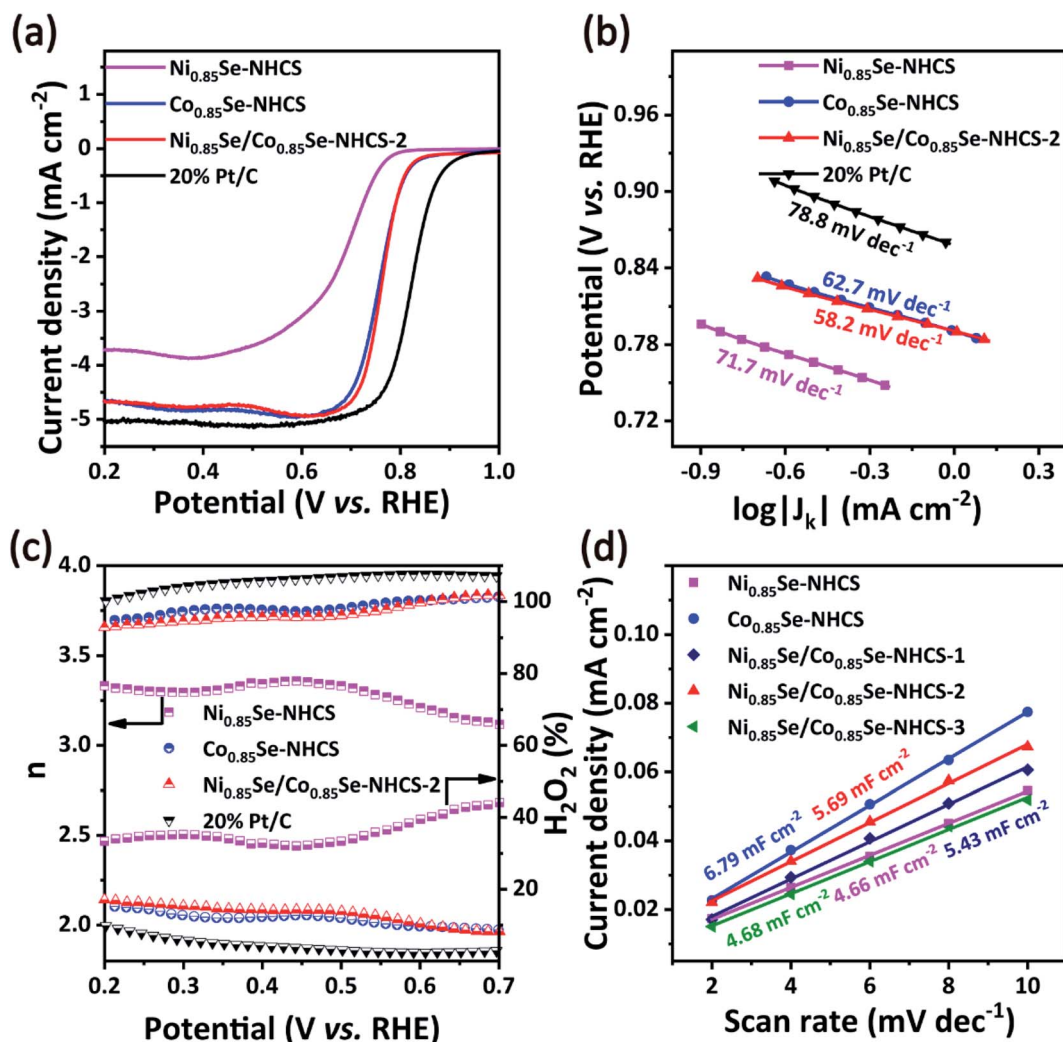
Fig. 5 (a) Linear sweep voltammogram curves for ORR and corresponding (b) Tafel curves, (c) converted electron transfer number and hydrogen peroxide yield of $Ni_{0.85}Se$-NHCS, $Ni_{0.85}Se$-NHCS, $Co_{0.85}Se/Ni_{0.85}Se$-NHCS-2, and 20% Pt/C. (d) The ECSA of synthesized samples by CV measurement in different scan rates.

0.69 V and $J_L = 3.71$ mA cm^{-2}). Obviously, the ORR performance of the $Ni_{0.85}Se/Co_{0.85}Se$-NHCS-2 mixture was mainly derived from the high content of Co^{2+} in $Co_{0.85}Se$-NHCS. Interestingly, the ORR activities of $Ni_{0.85}Se/Co_{0.85}Se$-NHCS-2 were better than that of 50% Ni-$Co_{0.85}Se$-NHCS (Fig. S9a†), which was prepared from $CoCl_2 \cdot 6H_2O$ and $NiCl_2 \cdot 6H_2O$ by co-precipitation. This result indicated that the catalyst prepared by the simple physical mixing method performed better than that prepared by the complex chemical method. As shown in Fig. 5b, the Tafel slope of $Ni_{0.85}Se/Co_{0.85}Se$-NHCS-2 was 58.2 mV dec^{-1}, lower than that of $Co_{0.85}Se$-NHCS (62.7 mV dec^{-1}), $Ni_{0.85}Se$-NHCS (71.7 mV dec^{-1}), 50% Ni-$Co_{0.85}Se$-NHCS (60.0 mV dec^{-1}) and 20% Pt/C (78.8 mV dec^{-1}), suggesting a faster kinetics rate of ORR process. Besides, electrochemical impedance spectroscopy (EIS) of these as-prepared catalysts was provided in Fig. S8.† According to the semicircle in the high-frequency region, the charge transfer resistance of $Ni_{0.85}Se/Co_{0.85}Se$-NHCS-2 was 3.68 Ω, between $Co_{0.85}Se$-NHCS (3.3 Ω) and $Ni_{0.85}Se$-NHCS (4.81 Ω), which was consistent with the fact that $Ni_{0.85}Se/Co_{0.85}Se$-NHCS-

2 was a mixture of $Ni_{0.85}Se$-NHCS and $Co_{0.85}Se$-NHCS. Furthermore, the detailed data of LSV curves and Tafel slopes of these catalysts were shown in Fig. S9 and Table S1.† The $Ni_{0.85}Se/Co_{0.85}Se$-NHCS-2 had the highest ORR activity among the mixtures with different mass ratios. Moreover, its activity was even higher than that of some nickel-cobalt-selenides reported in the literature (Table S2†). Remarkably, $Ni_{0.85}Se/Co_{0.85}Se$-NHCS-2 achieved the same ORR performance as $Co_{0.85}Se$-NHCS with only half the cobalt content. And with the mass ratio changed, the ORR performance of the mixtures decreased significantly. Therefore, it can be reasonably inferred that there is a synergistic effect between $Co_{0.85}Se$-NHCS and $Ni_{0.85}Se$-NHCS, which can affect the ORR activity of the mixture.

The electron transfer number (n) and H_2O_2 yields in the ORR process were carried out from the rotating ring-disk electrode (RRDE) measurement (Fig. 5c). The average n value evaluated for $Ni_{0.85}Se/Co_{0.85}Se$-NHCS-2 was 3.75, higher than that of $Ni_{0.85}Se$-NHCS (3.35), and closed to that of $Co_{0.85}Se$-NHCS (3.76) and noble metal catalyst 20% Pt/C (3.88), suggesting a four-

electron reaction process. Moreover, the H_2O_2 yield of $Ni_{0.85}Se/Co_{0.85}Se$-NHCS-2 was less than 12% in the voltage range from 0.2 to 0.7 V, lower than that of the $Co_{0.85}Se$-NHCS (13%) and commercial catalyst 20% Pt/C (8%). This result of $Ni_{0.85}Se/Co_{0.85}Se$-NHCS-2 further confirmed its excellent selectivity for ORR activity. For measuring the electrochemical surface area (ECSA), the double-layer capacitance (C_{dl}) was conducted by cyclic voltammetry at a scan rate from 2 mV s^{-1} to 10 mV s^{-1}. The CV curves of the as-prepared catalysts were shown in Fig. S10.† As shown in Fig. 5d, the C_{dl} of the $Ni_{0.85}Se/Co_{0.85}Se$-NHCS-2 was 5.69 mF cm^{-2}, which was second only to that of $Co_{0.85}Se$-NHCS and higher than that of other catalysts. This result demonstrates that the $Ni_{0.85}Se/Co_{0.85}Se$-NHCS-2 has a superior active surface area and active site for electrochemical activity. Besides, the super methanol tolerance was displayed in Fig. S11,† which was carried out the chronoamperometric test at 0.3 V in O_2-saturated 0.1 M KOH solution with 1600 rpm. The ORR activity of $Ni_{0.85}Se/Co_{0.85}Se$-NHCS-2 didn't change obviously after injecting 1 M methanol, while that of 20% Pt/C decreased evidently. It indicates that $Ni_{0.85}Se/Co_{0.85}Se$-NHCS-2 has outstanding methanol tolerance and a wide practical range. As shown in Fig. S12,† the limiting current density of $Ni_{0.85}Se/Co_{0.85}Se$-NHCS-2 only declined by 4.05% after 20 hours. By contrast, that of 20% Pt/C dropped off 13.14%. The above measurements result that $Ni_{0.85}Se/Co_{0.85}Se$-NHCS-2 has

excellent ORR performance, good methanol resistance, and remarkable stability, which is derived from the synergistic effect of $Ni_{0.85}Se$, $Co_{0.85}Se$, and NHCS.

The excellent cathodic catalysts of the zinc–air battery should possess outstanding bifunctional electrocatalysis for both ORR and OER. The OER performance of the prepared catalysts was analyzed in a three-electrode cell in 0.1 M KOH electrolyte and compared with other catalysts including the noble metal catalyst RuO_2. The operating potential at a current density of 10 mA cm^{-2} was used to evaluate the OER electrocatalytic activity of the material. As shown in Fig. 6a, the operating potential of $Ni_{0.85}Se/Co_{0.85}Se$-NHCS-2 was 1.63 V. It is a little worse than that of precious metal RuO_2 (1.59 V), close to that of $Ni_{0.85}Se$-NHCS (1.62 V), but better than that of $Co_{0.85}Se$-NHCS (1.65 V). Fig. 6b showed the Tafel slopes of these catalysts for OER. The $Ni_{0.85}Se/Co_{0.85}Se$-NHCS-2 exhibited a lower Tafel slope of 118.3 mV dec^{-1} than that of $Co_{0.85}Se$-NHCS (141.6 mV dec^{-1}), $Ni_{0.85}Se$-NHCS (136.0 mV dec^{-1}), and only higher than that of RuO_2 (84.1 mV dec^{-1}). Besides, the LSV curves and Tafel slopes of other mixed catalysts were also shown in Fig. S9 and Table S1.† The OER performance of $Ni_{0.85}Se/Co_{0.85}Se$-NHCS-2 with less Ni content was similar to that of $Ni_{0.85}Se$-NHCS, and higher than that of the mixtures with other mass ratios. Moreover, to further evaluate the intrinsic performance for OER of the catalysts, the TOF of catalysts was evaluated. $Ni_{0.85}Se/$

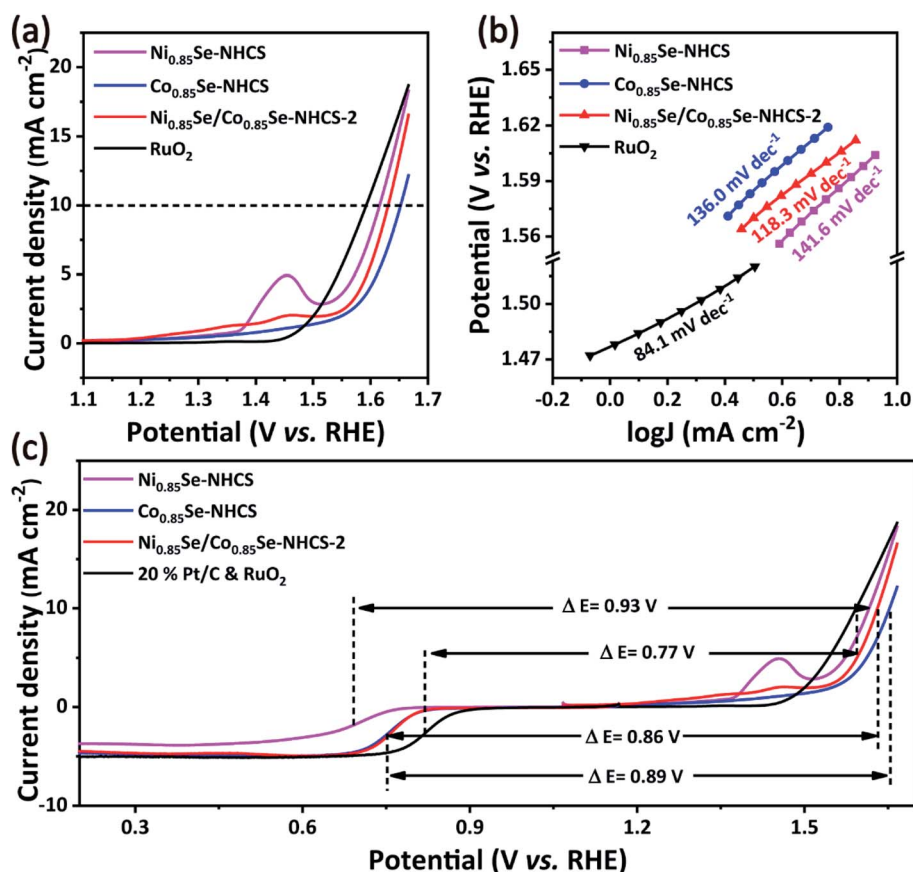Fig. 6 Linear sweep voltammogram curves for (a) OER and corresponding (b) Tafel slope curves, (c) the potential difference (ΔE) between $E_{1/2}$ for ORR and $E_{j=10}$ for OER.
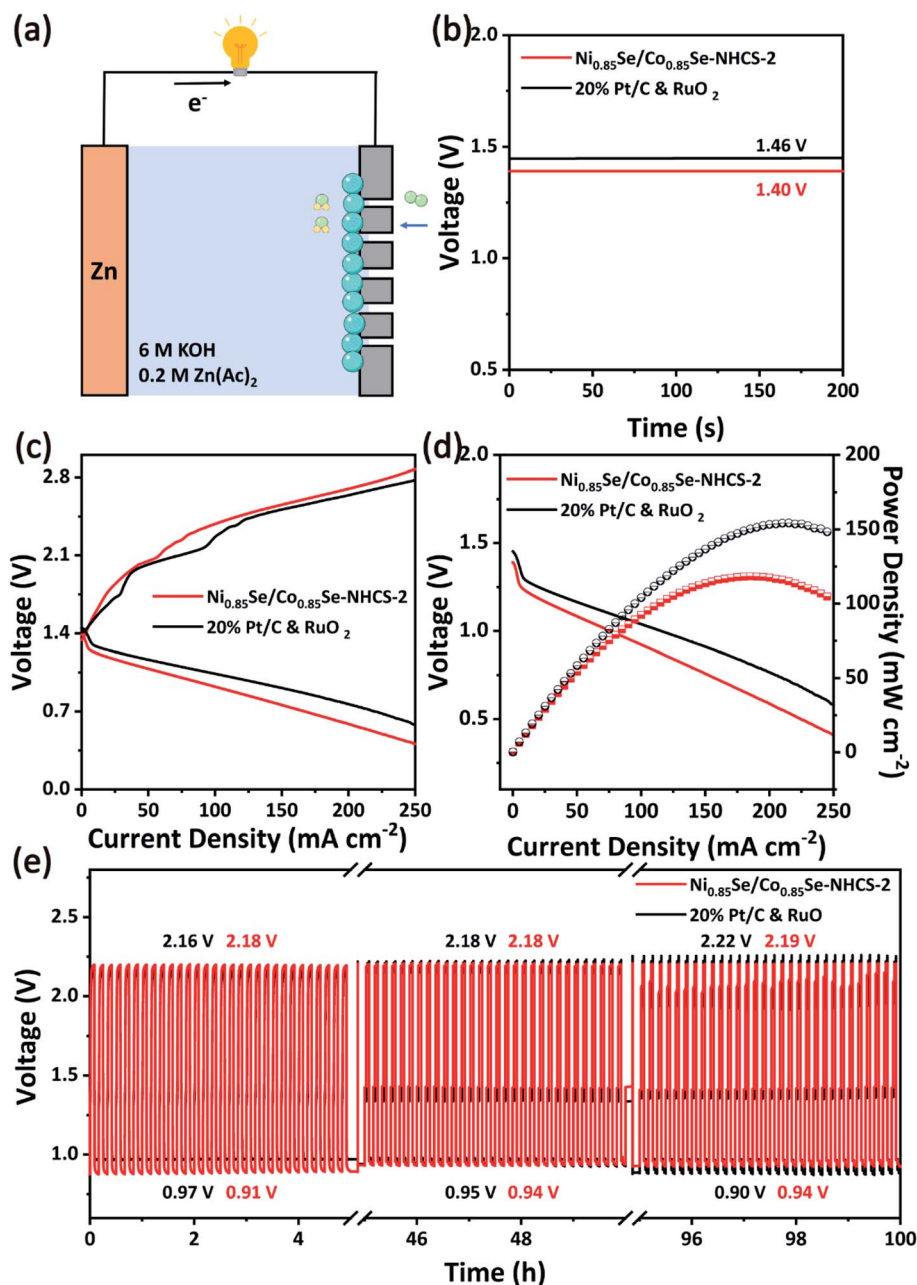
Fig. 7 (a) the schematic of the zinc–air battery. (b) The open-circuit curves, (c) charge and discharge polarization curves, (d) discharge polarization curves and corresponding the power density curves and the long-term stability by charge and discharge at 25 mA cm^{-2} of zinc–air battery assemble with Ni$_{0.85}$Se/Co$_{0.85}$Se-NHCS-2 and 20% Pt/C&RuO$_2$.

Co$_{0.85}$Se-NHCS-2 was calculated as 0.40 s^{-1} at the potential of 1.58 V, lower than that of Ni$_{0.85}$Se-NHCS (0.73 s^{-1}) and higher than that of Co$_{0.85}$Se-NHCS (0.26 s^{-1}), which demonstrated the OER activity of the mixed catalyst Ni$_{0.85}$Se/Co$_{0.85}$Se-NHCS-2 was mainly derived from the Ni$_{0.85}$Se-NHCS. Like the ORR performance, the Ni$_{0.85}$Se/Co$_{0.85}$Se-NHCS-2 with the rich of Ni^{3+} displayed a better OER performance than that of the other metal selenide materials (Table S2†). Furthermore, the potential difference (ΔE) between half-wave potential ($E_{1/2}$) for ORR and OER potential at 10 mA cm^{-2} ($E_{j=10}$) was applied to evaluate the performance of the bifunctional catalytic activity. The Ni$_{0.85}$Se/

Co$_{0.85}$Se-NHCS-2 illustrated a ΔE value of 0.86 V, which was lower than that of Co$_{0.85}$Se-NHCS (0.89 V), Ni$_{0.85}$Se-NHCS (0.93 V), indicating that Ni$_{0.85}$Se/Co$_{0.85}$Se-NHCS-2 possesses the optimum bifunctional ORR and OER performance among the non-precious metal catalysts (Fig. 6c). From the above results, it is shown that the Ni$_{0.85}$Se-NHCS-2 as a mixture of Ni^{3+}-rich Ni$_{0.85}$Se-NHCS and Co^{2+}-rich Co$_{0.85}$Se-NHCS has good ORR and OER bifunctional electrochemical activity when the same catalyst mass is used.

Due to the superior bifunctional activity of Ni$_{0.85}$Se/Co$_{0.85}$Se-NHCS-2, the zinc–air battery was assembled with this mixture as

cathode catalyst, zinc foil as an anode, and 6 M KOH and 0.2 M $Zn(Ac)_2$ as the electrolyte, respectively (Fig. 7a). The oxygen cathode in the zinc–air battery was made by coating the catalyst on carbon paper with a coating area of 1 cm^2. Moreover, the 20% Pt/C and RuO_2 noble metal mixture with a mass ratio of 1 : 1 was used as a comparison. As shown in Fig. 7b, the zinc–air battery equipped with $Ni_{0.85}Se/Co_{0.85}Se$-NHCS-2 exhibited the open potential of 1.40 V, coming near that of the battery with Pt/C&RuO_2 (1.46 V). Besides, the zinc–air battery based on $Ni_{0.85}Se/Co_{0.85}Se$-NHCS-2 worked and successfully drived a timer, testifying to the potential application of this catalyst in Fig. S13.† To further assess the performance of zinc–air devices, the charge and discharge curves were carried in Fig. 7c. The $Ni_{0.85}Se/Co_{0.85}Se$-NHCS-2 based battery exhibited a potential gap in charge and discharge measure approaching that of 20% Pt/C&RuO_2, which pointed out the awesome charge and discharge ability of the $Ni_{0.85}Se/Co_{0.85}Se$-NHCS-2 based battery. Moreover, the $Ni_{0.85}Se/Co_{0.85}Se$-NHCS-2 based battery was manifested a power density of 118.34 mW cm^{-2} at a current density of 185.1 mA cm^{-2}, while that of 20% Pt/C&RuO_2 achieved 154.13 mW cm^{-2} at 210.10 mA cm^{-2} (Fig. 7d). Moreover, the performance of zinc–air batteries with other non-precious catalysts was compared in Table S3.† To further appraise the practical stability application, the long-term charge and discharge activity of the $Ni_{0.85}Se/Co_{0.85}Se$-NHCS-2 and 20% Pt/C&RuO_2 was implemented at a current density of 25 mA cm^{-2} with 10 min per cycle. As exhibited in Fig. 7e, the zinc–air battery based on $Ni_{0.85}Se/Co_{0.85}Se$-NHCS-2 displayed better long-term stability through long cycle charging and discharging than that with 20% Pt/C&RuO_2. The potential gap of the $Ni_{0.85}Se/Co_{0.85}Se$-NHCS-2 based battery manifested a subtle change from 1.27 to 1.25 V after 100 hours due to the balanced concentration of dissolved oxygen, which was consistent with previous literature.[9,10] In particular, the $Ni_{0.85}Se/Co_{0.85}Se$-NHCS-2 based battery showed a slight increase in charging potential from 2.18 V to 2.19 V, which confirmed the excellent long-term stability of the OER. For comparison, the Pt/C&RuO_2 based battery performed an initial voltage gap of 1.19 V. But after 100 operation hours, the voltage gap changed to 1.32 V, suggesting the performance of the zinc–air battery obviously deteriorated. It can be seen that although the charge and discharge performance of $Ni_{0.85}Se/Co_{0.85}Se$-NHCS-2 based battery is slightly worse than that of Pt/C&RuO_2 based battery, it has better long-term stability. Considering the low cost of the non-precious metal catalyst, the $Ni_{0.85}Se/Co_{0.85}Se$-NHCS-2 has the potential to replace precious metals for zinc–air batteries.

Conclusions

In summary, we synthesized $Ni_{0.85}Se$-NHCS and $Co_{0.85}Se$-NHCS, respectively, by hydrothermal modification of $Ni_{0.85}Se$ and $Co_{0.85}Se$ nanoparticles on NHCS. The mixture $Ni_{0.85}Se/Co_{0.85}Se$-NHCS-2, which was prepared by simple mixing of $Ni_{0.85}Se$-NHCS and $Co_{0.85}Se$ in a 1 : 1 mass ratio, exhibited better ORR and OER bifunctionality than the single $Ni_{0.85}Se$-NHCS and $Co_{0.85}Se$-NHCS. The zinc–air battery equipped with $Ni_{0.85}Se/Co_{0.85}Se$-NHCS-2 performed more durable than the battery

equipped with the 20% Pt/C&RuO_2 catalysts. These results identify the rational mixture of nickel selenide and cobalt selenide as a simple, low-cost and efficient method for the preparation of oxygen electrode catalysts, further improving the performance and application prospect of zinc–air batteries.

Author contributions

Li-Juan Peng: conceptualization, investigation, writing – original draft. Jie-Ping Huang: investigation, data curation. Qiu-Ren Pan: validation, formal analysis. Ying Liang: investigation. Na Yin: investigation. Hang-Chang Xu: investigation. Nan Li: conceptualization, supervision, writing – original draft, project administration.

Conflicts of interest

The authors declare that they have no known competing financial interests or personal relationships that could have appeared to influence the work reported in this paper.

Acknowledgements

References

1 C. Wei, R. R. Rao, J. Peng, B. Huang, I. E. L. Stephens, M. Risch, Z. J. Xu and Y. Shao-Horn, *Adv. Mater.*, 2019, **31**, 1806296.

2 Z. W. Seh, J. Kibsgaard, C. F. Dickens, I. Chorkendorff, J. K. Norskov and T. F. Jaramillo, *Science*, 2017, **355**, 146.

3 X. X. Wang, M. T. Swihart and G. Wu, *Nat. Catal.*, 2019, **2**, 578–589.

4 J. Pan, Y. Y. Xu, H. Yang, Z. Dong, H. Liu and B. Y. Xia, *Adv. Sci.*, 2018, **5**, 1700691.

5 T. Sharifi, E. Gracia-Espino, A. Chen, G. Hu and T. Wågberg, *Adv. Energy Mater.*, 2019, **10**, 1902084.

6 S. Ren, X. Duan, S. Liang, M. Zhang and H. Zheng, *J. Mater. Chem. A*, 2020, **8**, 6144–6182.

7 A. Kulkarni, S. Siahrostami, A. Patel and J. K. Norskov, *Chem. Rev.*, 2018, **118**, 2302–2312.

8 M. Busch, N. B. Halck, U. I. Kramm, S. Siahrostami, P. Krtil and J. Rossmeisl, *Nano Energy*, 2016, **29**, 126–135.

9 S. Li, C. Cheng, X. Zhao, J. Schmidt and A. Thomas, *Angew. Chem., Int. Ed.*, 2018, **57**, 1856–1862.

10 A. I. Douka, Y. Xu, H. Yang, S. Zaman, Y. Yan, H. Liu, M. A. Salam and B. Y. Xia, *Adv. Mater.*, 2020, **32**, 2002170.

11 W. Xie, Z. Li, S. Jiang, J. Li, M. Shao and M. Wei, *Chem. Eng. J.*, 2019, **373**, 734–743.

12 D. Ding, K. Shen, X. Chen, H. Chen, J. Chen, T. Fan, R. Wu and Y. Li, *ACS Catal.*, 2018, **8**, 7879–7888.

13 S. Dou, X. Li, L. Tao, J. Huo and S. Wang, *Chem. Commun.*, 2016, **52**, 9727–9730.

14 Z.-q. Cao, M.-z. Wu, H.-b. Hu, G.-j. Liang and C.-y. Zhi, *NPG Asia Mater.*, 2018, **10**, 670–684.

15 Y. Zhang, H. Sun, Y. Qiu, X. Ji, T. Ma, F. Gao, Z. Ma, B. Zhang and P. Hu, *Carbon*, 2019, **144**, 370–381.

16 X. Duan, N. Pan, C. Sun, K. Zhang, X. Zhu, M. Zhang, L. Song and H. Zheng, *J. Energy Chem.*, 2021, **56**, 290–298.

17 X. Duan, S. Ren, N. Pan, M. Zhang and H. Zheng, *J. Mater. Chem. A*, 2020, **8**, 9355–9363.

18 L.-P. Lv, P. Du, P. Liu, X. Li and Y. Wang, *ACS Sustainable Chem. Eng.*, 2020, **8**, 8391–8401.

19 S. Wang, P. He, L. Jia, M. He, T. Zhang, F. Dong, M. Liu, H. Liu, Y. Zhang, C. Li, J. Gao and L. Bian, *Appl. Catal., B*, 2019, **243**, 463–469.

20 S. Liu, Y. Jiang, M. Yang, M. Zhang, Q. Guo, W. Shen, R. He and M. Li, *Nanoscale*, 2019, **11**, 7959–7966.

21 J. Ding, S. Ji, H. Wang, V. Linkov and R. Wang, *J. Power Sources*, 2019, **423**, 1–8.

22 J. Dai, D. Zhao, W. Sun, X. Zhu, L.-J. Ma, Z. Wu, C. Yang, Z. Cui, L. Li and S. Chen, *ACS Catal.*, 2019, **9**, 10761–10772.

23 X. Zheng, X. Han, Y. Cao, Y. Zhang, D. Nordlund, J. Wang, S. Chou, H. Liu, L. Li, C. Zhong, Y. Deng and W. Hu, *Adv. Mater.*, 2020, **32**, 2000607.

24 K. Karthick, S. N. Jagadeesan, P. Kumar, S. Patchaiammal and S. Kundu, *Inorg. Chem.*, 2019, **58**, 6877–6884.

25 Y. Huang, Z. Wang, Y. Jiang, S. Li, Z. Li, H. Zhang, F. Wu, M. Xie, L. Li and R. Chen, *Nano Energy*, 2018, **53**, 524–535.

26 S. Li, S. Peng, L. Huang, X. Cui, A. M. Al-Enizi and G. Zheng, *ACS Appl. Mater. Interfaces*, 2016, **8**, 20534–20539.

27 Q.-R. Pan, S.-J. Li, K. Tong, C. Xie, L. Peng, N. Li, D.-Y. Wang and H. Su, *J. Mater. Sci.*, 2019, **54**, 9063–9074.

28 L. Gui, Z. Huang, D. Ai, B. He, W. Zhou, J. Sun, J. Xu, Q. Wang and L. Zhao, *Chem.–Eur. J.*, 2020, **26**, 4063.

29 T. Meng, J. Qin, S. Wang, D. Zhao, B. Mao and M. Cao, *J. Mater. Chem. A*, 2017, **5**, 7001–7014.

30 P. Xu, J. Zhang, Z. Ye, Y. Liu, T. Cen and D. Yuan, *Appl. Surf. Sci.*, 2019, **494**, 749–755.

31 X. Hong, Y. Xu, R. Wang, P. Du, Z. Zhao, K. Huang, H. Tang, Y. Liu, M. Lei and H. Wu, *Adv. Mater. Interfacesc*, 2020, **7**, 2000740.

32 S. Ibraheem, S. Chen, L. Peng, J. Li, L. Li, Q. Liao, M. Shao and Z. Wei, *Appl. Catal., B*, 2020, **265**, 118569.

33 Y. Sun, K. Xu, Z. Wei, H. Li, T. Zhang, X. Li, W. Cai, J. Ma, H. J. Fan and Y. Li, *Adv. Mater.*, 2018, **30**, 1802121.

34 X. Zhao, X. Li, Y. Yan, Y. Xing, S. Lu, L. Zhao, S. Zhou, Z. Peng and J. Zeng, *Appl. Catal., B*, 2018, **236**, 569–575.

35 C. Huang, T. Ouyang, Y. Zou, N. Li and Z.-Q. Liu, *J. Mater. Chem. A*, 2018, **6**, 7420–7427.

36 D. Guo, R. Shibuya, C. Akiba, S. Saji, T. Kondo and J. Nakamura, *Science*, 2016, **351**, 361–365.

37 L. Yang, J. Shui, L. Du, Y. Shao, J. Liu, L. Dai and Z. Hu, *Adv. Mater.*, 2019, **31**, 1804799.

38 S. Kukunuri, M. R. Krishnan and S. Sampath, *Phys. Chem. Chem. Phys.*, 2015, **17**, 23448–23459.

39 C. Liu, K. Wang, X. Zheng, X. Liu, Q. Liang and Z. Chen, *Carbon*, 2018, **139**, 1–9.

40 W. Shi, X. Zhang and G. Che, *Int. J. Hydrogen Energy*, 2013, **38**, 7037–7045.

41 X. Sun, N. Habibul and H. Du, *Chin. J. Catal.*, 2021, **42**, 235–243.

42 Y. Zhang, Y. Qiu, X. Ji, T. Ma, Z. Ma and P. A. Hu, *ChemSusChem*, 2019, **12**, 3792–3800.

43 W. Zhao, S. Wang, C. Feng, H. Wu, L. Zhang and J. Zhang, *ACS Appl. Mater. Interfaces*, 2018, **10**, 40491–40499.

44 D. Lyu, Y. Du, S. Huang, B. Y. Mollamahale, X. Zhang, S. W. Hasan, F. Yu, S. Wang, Z. Q. Tian and P. K. Shen, *ACS Appl. Mater. Interfaces*, 2019, **11**, 39809–39819.

45 N. Zhang, Y. Wang, M. Jia, Y. Liu, J. Xu, L. Jiao and F. Cheng, *Chem. Commun.*, 2018, **54**, 1205–1208.

46 C. Li, X. Han, F. Cheng, Y. Hu, C. Chen and J. Chen, *Nat. Commun.*, 2015, **6**, 7345.

47 C. Li, W. Yuan, C. Li, H. Wang, L. Wang, Y. Liu and N. Zhang, *Chem. Commun.*, 2021, **57**, 4319–4322.

48 S. H. Lee, J. Kim, D. Y. Chung, J. M. Yoo, H. S. Lee, M. J. Kim, B. S. Mun, S. G. Kwon, Y. E. Sung and T. Hyeon, *J. Am. Chem. Soc.*, 2019, **141**, 2035–2045.

49 M. Zhu, Y. Yan, Q. Yan, J. Yin, K. Cheng, K. Ye, K. Zhu, J. Yan, D. Cao and G. Wang, *Int. J. Hydrogen Energy*, 2020, **45**, 10486–10493.

50 B. Yu, Y. Hu, F. Qi, X. Wang, B. Zheng, K. Liu, W. Zhang, Y. Li and Y. Chen, *Electrochim. Acta*, 2017, **242**, 25–30.

51 Z. Jin, M. Zhang, M. Wang, C. Feng and Z.-S. Wang, *J. Power Sources*, 2018, **378**, 475–482.

52 Z. Lin, C. Wang, Z. Wang, Q. Liu, C. Le, B. Lin and S. Chen, *Electrochim. Acta*, 2019, **294**, 142–147.

53 S. Wu, Q. Hu, T. Cui, H. Zhang, Q. Su, Y. Wang, Y. Xue, L. Wu and Q. Yang, *Synth. Met.*, 2020, **268**, 116499.

54 Y. Zhu, X. Yun, J. Li, K. Xiang, L. Xiao, H. Chen and X. Chen, *J. Electrochem. Soc.*, 2018, **165**, 3723–3731.

55 B. Yu, F. Qi, Y. Chen, X. Wang, B. Zheng, W. Zhang, Y. Li and L. C. Zhang, *ACS Appl. Mater. Interfaces*, 2017, **9**, 30703–30710.

56 X. Zheng, X. Han, H. Liu, J. Chen, D. Fu, J. Wang, C. Zhong, Y. Deng and W. Hu, *ACS Appl. Mater. Interfaces*, 2018, **10**, 13675–13684.

57 Y. Shi, W. Du, W. Zhou, C. Wang, S. Lu, S. Lu and B. Zhang, *Angew. Chem., Int. Ed.*, 2020, **59**, 22470–22474.